CrossMark

ORIGINAL PAPER

Otolith biochronologies reveal latitudinal differences in growth of Bering Sea yellowfin sole *Limanda aspera*

Mary Elizabeth Matta[1] · Thomas E. Helser[1] · Bryan A. Black[2]

Abstract Annual growth patterns in the hard parts of marine organisms are often related to factors in the physical environment; investigators are increasingly borrowing methods from the field of dendrochronology (tree-ring science) to explore these relationships. When applied to otoliths of yellowfin sole *Limanda aspera*, an abundant and commercially important flatfish, this approach has demonstrated a strong positive correlation between otolith growth and bottom temperature in the southeastern Bering Sea. In the present study, we assess whether the biochronology–growth relationship extends to yellowfin sole collected at higher latitudes. Two new northern Bering Sea biochronologies, one from the Bering Strait region and one near St. Matthew Island, were developed and compared with the southeastern Bering Sea biochronology using mixed effects modeling. Despite large distances (up to 600 km), a high degree of synchrony was observed among all three chronologies. However, subtle differences in growth among the three regions were revealed upon closer examination. The relative amplitude of otolith growth differed among the three chronologies, with stronger negative anomalies in the south and stronger positive anomalies in the north. Differences in average length at age were also detected, with fish growing slower to greater lengths at higher latitudes. Lastly, the Bering Strait

biochronology had the weakest and most localized relationships with climate variables, suggesting effects of climate may not be felt uniformly across the regions examined. Biochronologies may thus provide a useful tool in evaluating potential biological responses to projected climate change across a species' range.

Keywords Biochronology · Flatfish · Fish otoliths · Growth · Alaska

Introduction

Global temperatures have increased significantly over the past century, with some of the largest impacts being felt in the northern latitudes (IPCC 2014). Further warming is expected to continue such that the summer Arctic may be nearly sea-ice-free as early as 2040, according to climate model projections (Overland and Wang 2013; IPCC 2014). How these changes may affect ecosystem structure and function remains highly uncertain, though understanding relationships between long-term environmental records and biological responses may provide some insight. Such analyses ideally span a range of historical variability including regime shifts and extreme events and involve multiple species, trophic levels, or locations. However, in marine systems multi-decadal observational data are rare, especially for biological phenomena.

To address these limitations and generate long-term indices of climate effects on growth, techniques from tree-ring science (dendrochronology) have been applied to carbonate or siliceous parts of fish, bivalves, and corals (Black et al. 2005; Helama et al. 2006; Black 2009; Carilli et al. 2010). These structures often contain visible growth increments which form yearly and are commonly used to

✉ Mary Elizabeth Matta
  beth.matta@noaa.gov

1 Resource Ecology and Fisheries Management Division, Alaska Fisheries Science Center, National Marine Fisheries Service, National Oceanic and Atmospheric Administration, 7600 Sand Point Way NE, Seattle, WA 98115, USA

2 University of Texas at Austin Marine Science Institute, 750 Channel View Drive, Port Aransas, TX 78973, USA

estimate ages for population dynamics modeling. Through dendrochronology methods, time series of growth-increment widths from individuals can be used to generate biochronologies that capture population-level growth anomalies, are annually resolved (one value per year), and exactly dated. Central to the dendrochronology approach is crossdating, which ensures that each increment is assigned the correct calendar year of formation. Crossdating is based on the assumption that growth is limited by one or more aspects of climate, and that as climate varies over time, it induces synchronous growth patterns in all individuals exposed to those climatic features. The synchronous growth patterns can then be matched among individuals to ensure that all increments have been correctly identified and placed in time. Such dating control facilitates the comparison of biochronologies with one another, instrumental climate records, or observational biological time series (Butler et al. 2010; Black et al. 2011; Gillanders et al. 2012; Black et al. 2014).

Recently, advanced statistical approaches such as mixed effects modeling (Morrongiello et al. 2012) and Bayesian methods (Helser et al. 2012) have been applied to biochronology data. These methods simultaneously evaluate intrinsic (e.g., age-dependent) and extrinsic (e.g., environmental or density-related) effects while allowing for quantification of uncertainty in variance components and model parameters (Weisberg et al. 2010; Helser et al. 2012; Morrongiello et al. 2012). Whereas methods that detrend time series individually are typically focused solely on extrinsic sources of variation, mixed effects models accommodate the hierarchical nature of growth-increment data and explain variation at the individual level as well as allow for assessment of interactions between an individual and its environment (Morrongiello and Thresher 2015).

Yellowfin sole (*Limanda aspera*), currently the target of the largest flatfish fishery in the world, is one of the most abundant species of flatfish in continental shelf waters of the North Pacific Ocean, ranging from British Columbia north into the Chukchi Sea and west to the Sea of Japan (Wilderbuer et al. 1992, 2015). Adult yellowfin sole are known to make seasonal migrations between the inner and outer continental shelves of the Bering Sea, occupying the outer shelf during the winter and moving to the middle and inner shelves in the spring and summer (Bakkala 1981; Wakabayashi 1989; Wilderbuer et al. 1992). Due to its diet elasticity and the presence in sub-Arctic waters, yellowfin sole may potentially expand its summer range north into the Arctic, where the projected loss of summer sea ice is expected to lead to increased primary productivity and prey for fish stocks (Hollowed et al. 2013).

The relative clarity of yellowfin sole's otolith increments makes it an ideal candidate for biochronology development. Indeed, an otolith biochronology from

yellowfin sole collected in the southeastern Bering Sea was successfully developed and was found to have a strongly positive correlation with ambient temperature ($r = 0.90$; Matta et al. 2010). Moreover, anomalies in the growth-increment biochronology were found to correspond to anomalies in age-specific body size, indicating a link between somatic and otolith growth (Black et al. 2013). Thus, otolith biochronologies for yellowfin sole could be expanded across a range of spatial scales to identify the degree to which long-term climate variability influences growth and provide some insight as to how the geography of those drivers may shift with continued warming.

Here, we develop two new yellowfin sole biochronologies from the northeastern Bering Sea for comparison with an existing southeastern Bering Sea biochronology (Matta et al. 2010). We hypothesize that temperatures should be more limiting to growth toward the northern limits of the species' range and that all biochronologies should share some degree of synchrony driven by basin-wide climate variability. Specific objectives were to (1) compare the three biochronologies of yellowfin sole and their climate responses along a latitudinal gradient in the Bering Sea, (2) assess the level of variability within and among biochronologies, and (3) identify intrinsic (inherent) and extrinsic (environmental) factors related to otolith growth. We used a linear mixed effects model to partition variability in the functional growth response recorded in otolith increments among fish age, collection site, year effects, and unexplained factors. Lastly, somatic body growth (i.e., length at age) was modeled for an expanded collection of yellowfin sole from the same region as each biochronology to identify potential latitudinal differences. Ultimately, the latitudinal gradients considered here may provide some indication of the shifts in ecological attributes and climate limitations of yellowfin sole in the Bering Sea as isotherms continue to migrate poleward.

Materials and methods

Otolith measurements and crossdating

Otoliths were collected during the summer 2010 bottom trawl survey in the northeastern Bering Sea, conducted by the Resource Assessment and Conservation Engineering (RACE) division of the Alaska Fisheries Science Center (AFSC). For details on survey methods, see Lauth (2011). Otoliths were collected in two distinct areas: (1) south of Bering Strait and (2) northeast of St. Matthew Island (Fig. 1), hereafter referred to as the Bering Strait and St. Matthew biochronologies, respectively. These were compared with an existing otolith biochronology (Matta et al.

Fig. 1 Map of the eastern Bering Sea, showing haul collection sites of yellowfin sole (*Limanda aspera*) used to develop otolith growth-increment biochronologies, mooring locations (M2, M4, and A2), and 50-m depth contours. Multiple fish were collected from the same haul in some cases
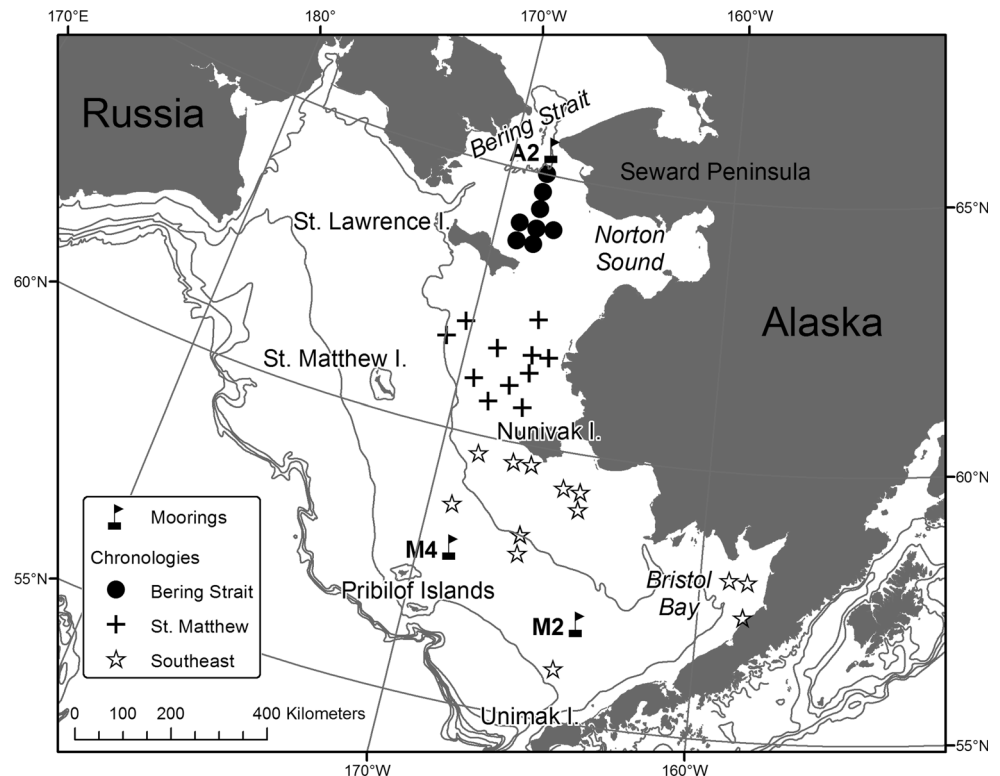
2010) from the southeast Bering Sea, hereafter referred to as the Southeast biochronology (Fig. 1).

In the laboratory, otoliths were transversely sectioned with a scalpel and burned over an ethanol flame to enhance the contrast between growth zones. Otoliths were photographed using a Leica[1] DFC420 digital camera attached to a Leica MZ95 microscope.

Calendar years were assigned to each growth increment via the process of crossdating, a central tenet of dendrochronology and necessary step in any biochronology analysis. Crossdating assumes that climate variability induces growth patterns that are shared among individuals in a given area. For example, anomalously low temperatures may cause growth-increment widths to be narrow and high temperatures may cause them to be wide relative to adjacent increments. Beginning with the increment formed during the known year of capture, these synchronous patterns, analogous to barcodes, can then be matched among individuals to ensure that all increments have been correctly identified. If a growth increment has been missed or falsely added, the growth pattern for that individual should be offset by 1 year, thereby indicating that a dating error has occurred. Only fish 14 years or older with clear otolith growth increments were included in the biochronology analysis to ensure adequate time series length. Fish ages

had previously been estimated by counting otolith growth zones as part of routine age determination for stock assessments by the AFSC's Age and Growth Program (Shockley and Matta 2012), which provided an opportunity to compare zone count and crossdated age estimates.

Following visual crossdating, growth-increment widths were measured to the nearest 0.0001 mm using Image-Pro Plus version 7.0 software (Media Cybernetics) based on methods described in Matta et al. (2010). The innermost 3–5 growth increments of each otolith were not measured due to rapid early ontogenetic changes in growth rates that distorted increment widths in the region of the measurement axis (Matta et al. 2010).

Visual crossdating was then statistically checked using the International Tree-Ring Data Bank Program Library software COFECHA (Holmes 1983; Grissino-Mayer 2001). The program was used to fit each individual growth-increment time series with a cubic smoothing spline with a 50 % wavelength cutoff set at 15 years. Observed growth-increment values were then divided by values predicted by the spline to isolate high-frequency (year-to-year) variability and standardize each series to a mean of one. Next, each individual detrended measurement time series was correlated with the mean of all others from time zero ±10 years. A substantially higher lagged correlation would indicate that a dating error may have occurred and that the sample should be visually re-examined. Individual time series with a nonsignificant ($p < 0.01$) correlation were

---

[1] Reference to trade names does not imply endorsement by the National Marine Fisheries Service, NOAA.

visually re-inspected for crossdating errors; however, at no point was crossdating forced on an otolith, and corrections were only made when accidentally missed or falsely added increments were easily identifiable. The detrending process described here was used solely to verify crossdating and identify dating errors; methods used to develop the biochronology for each of the three regions are described in the following section.

Two summary statistics were calculated for each of the three biochronologies: the series intercorrelation, which is the average correlation between each detrended measurement time series and the average of all others, and the average mean sensitivity, which describes the relative year-to-year change in growth-increment width across specimens within a region, with values ranging from 0 (a pair of increments of the same width) to 2 (a pair in which one width is 0; Fritts 1976).

Statistical model used to generate biochronologies

After all increments were correctly dated, a hierarchical mixed effects model was used to analyze otolith growth-increment data and generate biochronologies. Based on earlier studies modeling growth-increment data (Helser and Lai 2004; Helser et al. 2012), we chose the nonlinear exponential decay function to model growth-increment variation as a function of age at formation. Based on this assumed relationship, yellowfin sole otolith increment growth can be described as:

$$L_{ijk} = a_{j(k)} A_{ijk}^{b_j(k)}$$

where L is the growth-increment width, $i = 1, 2, \ldots, n_j$ growth increments of individual fish j and site k ($k = 1, 2, 3$ for the Bering Strait, St. Matthew, and southeast biochronologies, respectively) measured at age A. The parameters $a_{j(k)}$ and $b_{j(k)}$ are the y-axis intercept and exponential decay, respectively, of the function for each fish's otolith within each site. Data were linearized by log–log transformation of otolith growth-increment widths and increment ages, which served to stabilize the variance structure, where $y_{ijk} = \ln(L_{ijk})$, $x_{ijk} = \ln(A_{ijk})$, $\alpha_{j(k)} = \ln(a_{j(k)})$, and $\beta_{j(k)} = b_{j(k)}$. The linear mixed effects model accounting for intrinsic growth, random individual growth, and extrinsic environmental variation is specified as:

$$y_{ijk} = \left(\bar{\alpha}_k + \alpha_{j(k)}\right) + \left(\bar{\beta}_k + \beta_{j(k)}\right) x_{ijk} + \tau_{t,k} + e_{ijk}$$

where x_{ijk} is the age at formation of growth increment i of individual fish j and site k, $\bar{\alpha}_{jk}, \bar{b}_{jk}$ is the fixed (population average) intercept and slope, respectively, that describe the decline in growth-increment width as a function of age at formation for all individual fish specific to each site k, $\tau_{t,k}$ is

the random environmental (year-to-year) variation specific to year t and site k, and e_{ijk} is the residual error variance. Individual variation in the above relationship at each site k is expressed by the parameters $\alpha_{j(k)}, \beta_{j(k)}$ and modeled by assuming that $\boldsymbol{\varphi}_1 = \left(\alpha_{j(k)}, \beta_{j(k)}\right)'$ is a random draw from a multivariate normal distribution (*MVN*) with mean vector $\boldsymbol{\mu} = \left(\bar{\mu}_{\alpha 1}, \bar{\mu}_{\beta 1}, \bar{\mu}_{\alpha 2}, \bar{\mu}_{\beta 2}, \bar{\mu}_{\alpha 3}, \bar{\mu}_{\beta 3}\right)'$ and variance–covariance matrix $\mathbf{G} = \mathrm{diag}(\mathbf{G}_1, \mathbf{G}_2, \mathbf{G}_3)$, where $\mathbf{G}_k = \begin{bmatrix} \sigma_{\alpha,k}^2 & \sigma_{\alpha\beta,k} \\ \sigma_{\beta\alpha,k} & \sigma_{\beta,k}^2 \end{bmatrix}$ for $k = 1, 2, 3$ sites; in brief, $\boldsymbol{\varphi}_1 \sim \mathrm{MVN}(\boldsymbol{\mu}, \mathbf{G})$. The variance–covariance $\mathbf{G}_k$ is uncorrelated, independent, and unstructured 2×2 matrices. Year-to-year environmental effects $\tau_{t,k}$ are modeled as random draws from a normal distribution with a mean of zero and variance of $\sigma_{h,k}^2$ across T years (Weisberg et al. 2010), or $\tau_{t,k} \sim N\left(0, \sigma_{h,k}^2\right)$ for $t = 1, \ldots, T$ years and $k = 1, 2, 3$ sites. Helser et al. (2012) has shown that the coefficients τ from mixed effects models are equivalent to the method of biochronology development most commonly used in dendrochronology studies, in which measurement time series are individually detrended using negative exponential curves, cubic splines, or similar mathematical functions. However, coefficients from the mixed effects model have the advantage of capturing inherent individual variability in growth. This model can be equivalently described by $\tau_{t,k} = 0 + \varepsilon_2$ and $\varepsilon_2 \sim N\left(0, \sigma_{h,k}^2\right)$ for all years and sites. The residual error is assumed to be independent, normally distributed random variables, $e_{ijk} \sim N\left(0, \sigma_{e,k}^2\right)$. However, additional covariance structure addressing within-animal correlation may be specified and may be particularly useful for growth-increment data which represent a sort of time series. For simplicity, the first-order autocorrelation, or AR1 dependence, in the error e_{ijk} was assumed: $e_{ijk} = \rho_{jk} e_{i-1,jk} + u_{ijk}$, where $u_{ijk} \sim N\left(0, \sigma_{u,k}^2\right)$, ρ_{jk} is the correlation coefficient for the growth-increment time series of yellowfin sole j in site k, and subscript $i - 1$ indicates the age prior to age i.

We fit the model to the growth-increment data using restricted maximum likelihood implemented in the MIXED procedure in SAS (Statistical Analysis Institute). The full model described above (model 1) was compared to two other models with decreasing complexity; model 2 removed the environmental variance term ($\tau_{t,k}$), and model 3 additionally removed the site-specific fixed growth effects. The goal was to quantify the weight of evidence in support of intrinsic growth differences and extrinsic environmental effects from different regions in the Bering Sea, which were tested using the Akaike information criterion (AIC; Burnham and Anderson 2002). Support for a given

model was calculated based on AIC differences as $\Delta_i = \text{AIC}_i - \text{AIC}_{\min}$, where AIC_i is the AIC for the ith model and $\text{AIC}_{\min}$ is the minimum of AIC among all the models. Typically, models with $\Delta_i > 10$ have no support.

Fish length at age

To evaluate latitudinal differences in somatic growth, length-at-age data from a larger sample of fish from each area (southeast, St. Matthew, and Bering Strait) were fit with von Bertalanffy growth functions (von Bertalanffy 1938). All yellowfin sole collected during the 2010 AFSC RACE bottom trawl survey were considered in this analysis, using the following bounds for each area: southeast (55–60°N, 160–170°W), St. Matthew (60–62.5°N, 165–172°W), and Bering Strait (63.5–66°N, 165–170°N). Growth models were fit separately for males and females. The form of the growth function is:

$$l_{ij} = L_\infty(1 - e^{-K(t_i - t_0)}) + e_{ij}$$

where l_{ij} is the fish length in centimeters of the jth individual at age t_i ($i = 1,\ldots, m$), L_∞ is the asymptotic maximum length, K is a growth constant, t_0 is the age at which length would hypothetically be zero, and e_{ij}'s are independent identically distributed additive normal random $N(0, \sigma^2)$ variates. The model was fit to the data using the NLIN procedure in SAS, and regions were compared using the F ratio statistic from sums of squared errors using the equation:

$$F_R = \frac{(\text{SSE}_r - \text{SSE}_f)/q}{\text{SSE}_f/(n-p)} = \frac{(\text{SSE}_r - \text{SSE}_f)/q}{\text{SSE}_f}$$

where F_R is the F ratio statistic, SSE_r and SSE_f are the sums of squared residual errors for the reduced (all observations without respect to region) and full models (region-specific fits), respectively, n is the number of sample observations, p is the number of parameters, and q is the difference in parameters between the reduced and full models.

Correlations

The two new biochronologies (Bering Strait and St. Matthew) were compared to each other and to the existing Southeast biochronology using the Pearson correlation coefficient, r, over the common time period of 1989–2006. For each area, years with fewer than six individuals contributing were not included in the biochronology to ensure adequate signal-to-noise ratios (Matta et al. 2010).

Biochronologies were compared to climate indices from a variety of sources. As in Matta et al. (2010), biochronologies were compared to average summer bottom temperatures recorded during the AFSC RACE annual

eastern Bering Sea bottom trawl survey in the area 55–62°N, 158–179°W, and to the Ice Cover Index, defined as the average ice concentration for Jan 1–May 31 for the area 56–58°N, 163–165°W (NOAA 2014).

Time series of temperatures from mooring sites in the Bering Sea were also compared to the otolith biochronologies. Several sources of data were used, including the A2 mooring in the eastern channel of Bering Strait maintained since 1990 (Woodgate et al. 2005), the M4 mooring near the Pribilof Islands in the Bering Sea maintained since 1996, and the M2 mooring in the southeastern Bering Sea maintained since 1970 (Fig. 1). Temperatures measured near-bottom at each mooring (45, 61, and 65 m for the A2, M4, and M2 moorings, respectively) were averaged from the months of June through November to correspond to the main period of observed otolith deposition (Wakabayashi 1989; Kimura et al. 2007). Years without sufficient data (e.g., where moorings were not continuously recording) were excluded from analysis.

Gridded, monthly averaged Hadley sea surface temperatures (HadISST) with 1° spatial resolution (Rayner et al. 2003) were also correlated with the yellowfin sole biochronologies to corroborate results from the mooring data. First, each biochronology was correlated with monthly SST values including lags of ±4 months into adjacent years. Only months in which highly significant ($p < 0.01$) correlations occurred in the Bering Sea were retained. Values of SST were then averaged across highly significant months to generate a final correlation map for each chronology using the KNMI Climate Explorer (http://climexp.knmi.nl). Correlations significant at the relatively low threshold of $p < 0.10$ were displayed in the map to better highlight the spatial characteristics of the climate–biology relationships.

Results

Biochronology properties

A total of 44 fish collected near Bering Strait and 34 fish collected near St. Matthew were 14 years or older. Of these, 23 otoliths from each region had growth patterns that were adequately clear for obtaining accurate measurements and were used to develop the final biochronologies. Crossdating revealed that ages estimated by growth zone counts during routine age production were incorrect for 10 fish (five in each region). Age estimates differed by only 1 year for seven fish, 2 years for two fish, and 4 years for one fish. In general, the disparities between counted growth zones and ages based on crossdating were likely associated with difficulty in interpreting compressed zones or growth

at the otolith edge, common problems in routine age determination (Matta and Goetz 2012). Bering Strait fish ranged from 15 to 36 years in age, and St. Matthew fish ranged from 14 to 31 years in age (Table 1). Otolith increment measurements from the 21 individuals used to create the Southeast biochronology in Matta et al. (2010) ranged in age from 18 to 34 years.

Series intercorrelations were 0.57 for the Bering Strait biochronology, 0.53 for the St. Matthew biochronology, and 0.66 for the Southeast biochronology, indicating a high degree of synchrony among individuals within each site (Table 1). A high degree of synchrony was also apparent among sites as evidenced by significant correlations among the three biochronologies (Table 2). The strongest correlation was between the Bering Strait and St. Matthew biochronologies ($r = 0.86$; $p < 0.0001$), though somewhat weaker but still highly significant correlations ($p < 0.0001$) were found between the Southeast biochronology and the two northern biochronologies (Table 2).

Model results

The negative exponential function appeared to approximate the yellowfin sole otolith growth-increment data well. Individual time series of increment widths were quite variable over time with generally synchronous positive and negative trends among years (Fig. 2a–c). When sorted as a function of the age at which a particular growth increment was formed (Fig. 2d–f), the datasets mimicked the allometric change (intrinsic growth) in somatic body size relative to age commonly seen among marine organisms. While increment widths at age varied considerably among the individual fish, on average they all showed a coherent monotonic decline consistent with expected age-related changes in otolith accretion rate (Fig. 2).

The full model (model 1) accounting for region-specific fixed growth effects (α_k β_k), individual random growth effects ($\Sigma = \sigma^2_{\alpha,k}$, $\sigma^2_{\beta,k}$), and a random year-to-year term ($\sigma^2_{h,k}$) provided a substantially better fit to the growth-increment data than either model 2 or model 3 (Table 3).

Compared to the full model, the Δ_i was 396.6 and 453.3 for model 2 and model 3, respectively, which exceeds the value of 10 by a large margin. Values of β became more negative moving from the southeastern Bering Sea ($\beta = -0.364$) to the Bering Strait ($\beta = -0.464$), indicating a more rapid decline in increment width with respect to age in the northern part of the study region (Table 3). The variance of β ($\sigma^2_{\beta,k}$) was also considerably smaller in the southeastern Bering Sea ($\sigma^2_{\beta,3} = 0.020$) than in the two northerly regions, indicating the growth rate or age-related decline (change in growth-increment width) was more consistent across individual southeast otoliths measured (Table 3). Inclusion of unspecified year-to-year variability, $\sigma^2_{h,k}$, as a random effect in the model resulted in the greatest relative change in the Δ_i (453.3) among models. Model 1 represents an alternative to modeling growth as an explicit function of climate factors simply by treating year as a random effect, but this formulation lacks any specificity as to what climate factor might be an important growth predictor. Some authors have referred to $\sigma^2_{h,k}$ as an environmental variance term, but without explicitly modeling environmental factors on growth, it really expresses a combination of unknown annual effects. Here variance of annual growth-increment variability ($\sigma^2_{h,k}$) was greatest in the St. Matthew region (0.062), followed by Bering Strait and the southeast region. The random year term coefficients from the mixed effects model provide a measure of annual growth variability, which is explored with respect to climate variability below. We used the term "growth-increment index" as an integrative measure of interannual deviation in growth among individuals in the sample, since by definition the year effect coefficients $\tau_{t,k} \sim N\left(0, \sigma^2_{h,k}\right)$. Each region showed a degree of coherence in growth, as was also reflected by strong series intercorrelations (Table 1). Individual and environmental variability is captured in Fig. 3 which shows 95 % confidence intervals about each of the biochronologies. Again each region showed considerable consistency over years, particularly in 1999 and 2000 when growth was below

Table 1 Yellowfin sole (*Limanda aspera*) otolith growth-increment biochronology properties

Biochronology	n	Time period	Mean sensitivity	Series intercorrelation	Mean series length (years)
Bering Strait	23	1984–2008	0.27	0.57	20.9
St. Matthew	23	1988–2008	0.28	0.53	16.7
Southeast Bering Sea[a]	21	1989–2006	0.26	0.66	16.9

Mean sensitivity is an index of year-to-year variability, series intercorrelation is the average correlation between each detrended time series and the average of all other standardized time series, mean series length is the average length of the measurement time series used in the biochronology, time period is the range of years spanned by the biochronology, and n is the number of otoliths used to develop each biochronology

[a] From Matta et al. (2010)

Table 2 Correlation coefficients (r) for pairwise comparisons of 3 yellowfin sole (*Limanda aspera*) biochronologies (SE is Southeast, SM is St. Matthew, BS is Bering Strait) and time series of environmental indices

	SE	SM	BS	BT$_{survey}$	ICI	M2	M4	A2
SE	1	0.83***	0.76***	0.91***	−0.60**	0.71***	0.66	0.73**
SM		1	0.86***	0.72***	−0.44*	0.60**	0.71*	0.49
BS			1	0.68***	−0.40*	0.62***	0.55	0.41
BT$_{survey}$				1	−0.68***	0.74***	0.78*	0.75***
ICI					1	−0.72***	−0.63	−0.45
M2						1	0.58	0.50
M4							1	0.44
A2								1

BT$_{survey}$ is average bottom temperature from the summer AFSC RACE bottom trawl survey, ICI is ice cover index, and M2, M4, and A2 are near-bottom temperatures measured by Bering Sea mooring buoys located in the southern, central, and northern Bering Sea, respectively (averaged Jun–Nov)

Significant correlations are indicated by asterisks (* $p < 0.05$; ** $p < 0.01$; and *** $p < 0.001$)

Fig. 2 Raw otolith growth-increment (ring width) measurements for yellowfin sole (*Limanda aspera*) collected from **a** Bering Strait, **b** St. Matthew, and **c** southeast Bering Sea. Growth-increment width with respect to age at time of formation for the **d** Bering Strait, **e** St. Matthew, and **f** Southeast Bering Sea biochronologies. The *bottom* and *top* of *each box* represent the 25th and 75th percentiles, respectively, and the *horizontal band* within *each box* represents the median. The *lower* and *upper vertical bars* (whiskers) represent the 5th and 95th percentiles, respectively
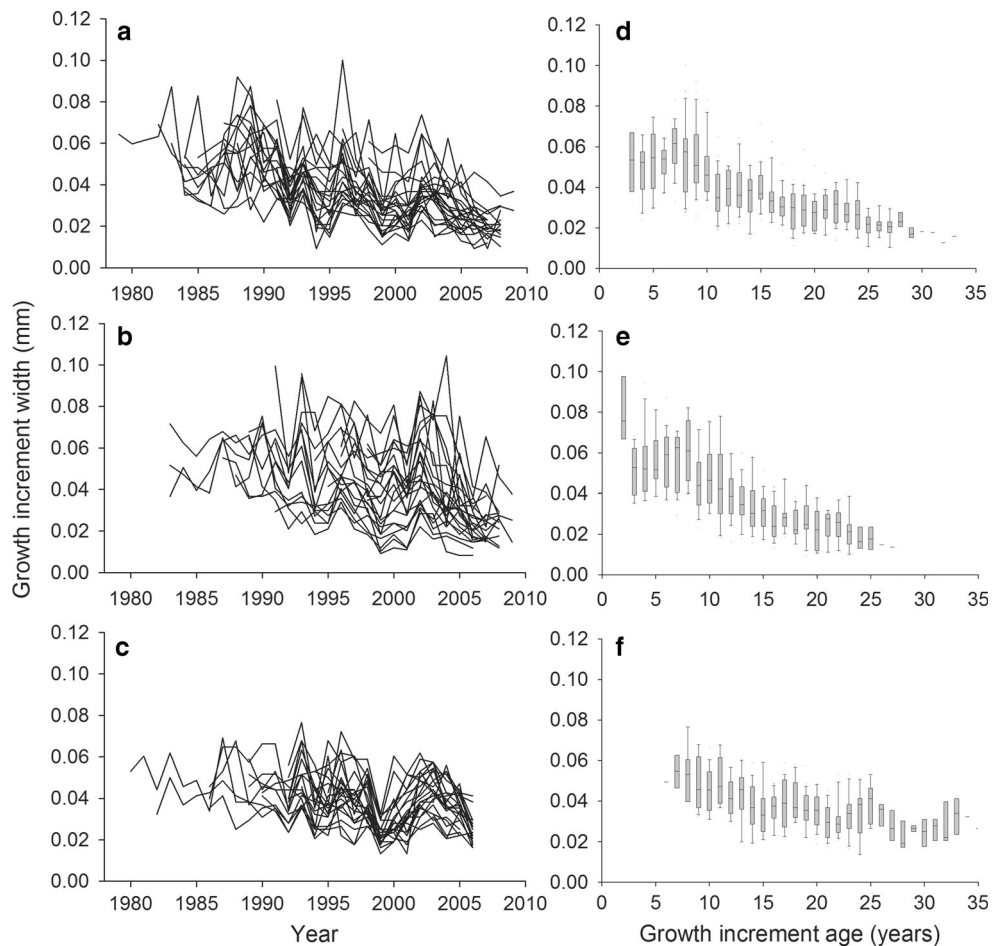
average, followed by above-average growth from 2002 through 2004 (Fig. 3).

Environmental relationships

The Southeast biochronology had the strongest relationship with average Bering Sea bottom temperatures measured during summer trawl surveys ($r = 0.91$, $p < 0.0001$), likely because the individuals used to develop this biochronology were from the same region. However, the Bering Strait and St. Matthew biochronologies were also significantly related to southern Bering Sea summer bottom temperatures (Table 2). Of the three biochronologies, the Southeast biochronology had the strongest negative

Table 3 Parameter and variance (σ^2) estimates from each of three models of yellowfin sole (*Limanda aspera*) otolith growth

Coefficient	Model 1		Model 2		Model 3	
	Mean	SD	Mean	SD	Mean	SD
$\bar{\alpha}_1$	−2.145	0.212	−1.860	0.205	−2.078	0.292
$\bar{\beta}_1$	−0.464	0.074	−0.575	0.074	−0.496	0.034
$\bar{\alpha}_2$	−2.257	0.246	−1.986	0.197	–	–
$\bar{\beta}_2$	−0.432	0.096	−0.556	0.077	–	–
$\bar{\alpha}_3$	−2.383	0.238	−2.469	0.224	–	–
$\bar{\beta}_3$	−0.364	0.069	−0.336	0.057	–	–
$\sigma^2_{\alpha,1}$	0.350		0.462		0.142	
$\sigma^2_{\beta,1}$	0.057		0.067		0.028	
$\sigma^2_{\alpha,2}$	0.444		0.237		–	
$\sigma^2_{\beta,2}$	0.118		0.064		–	
$\sigma^2_{\alpha,3}$	0.095		0.086		–	
$\sigma^2_{\beta,3}$	0.020		0.021		–	
$\sigma^2_{h,1}$	0.033		–		–	
$\sigma^2_{h,2}$	0.062		–		–	
$\sigma^2_{h,3}$	0.028		–		–	
$\sigma^2_{e,1}$	0.057		0.086		0.096	
$\sigma^2_{e,2}$	0.066		0.108		–	
$\sigma^2_{e,3}$	0.042		0.077		–	
AIC (Δ_i)	287.8 (0)		684.4 (396.6)		741.1 (453.3)	

Model 1 is the full model and accounts for additional site-specific growth effects ($\alpha_{j(k)}$, $\beta_{j(k)}$) and a random year effect (σ^2_h). Model 2 reduces complexity by removing random year effects, and model 3 further removes site-specific fixed growth effects. SD is the standard deviation of each mean parameter estimate. All models include individual random variation in otolith growth increments. Fixed effect parameters and variances subscripted as 1, 2, and 3 refer to the Bering Strait, St. Matthew, and Southeast, respectively. σ^2_h is the variance of the year effect models, and σ^2_e is unexplained error. Akaike information criterion identifies support for a given model, where AIC_i is the AIC for the *i*th model, AIC_{min} is the minimum of AIC among all the models, and $\Delta_i = AIC_i - AIC_{min}$. Typically, models with $\Delta_i > 10$ have no support

correlation with ice cover ($r = -0.60$, $p = 0.009$; Table 2). All three biochronologies were significantly related to near-bottom temperatures averaged for the months of Jun–Nov (corresponding to the primary period of otolith growth) at the southernmost mooring M2 (Table 2). However, the Bering Strait biochronology was not significantly correlated with Jun–Nov bottom temperatures measured at either M4 or A2 (Table 2).

Correlations between gridded SSTs and each biochronology demonstrated differences in correlation strength and spatiotemporal extent (Fig. 4). Months with highly significant ($p < 0.01$) correlations were sequential and included the period of known otolith deposition (Wakabayashi 1989; Kimura et al. 2007). For all three biochronologies, these highly significant correlations occurred beginning in April, but spanned a window through November (8 months) for the Bering Strait biochronology, the following March for the St. Matthew biochronology (12 months), and the following January for the Southeast biochronology (10 months). Correlations with average SST were generally the weakest for the

Bering Strait biochronology, while the St. Matthew and Southeast biochronologies were strongly related to temperature variability across the Bering Sea and even through the Gulf of Alaska (Fig. 4).

Somatic growth differences

During the 2010 trawl survey, 114 yellowfin sole were collected from the Bering Strait region, 229 were collected from the area near St. Matthew, and 615 were collected in the southeast region (Table 4). We observed significant differences in yellowfin sole somatic body growth as expressed by fits of the von Bertalanffy growth function to length-at-age data from each region (Table 4; Fig. 5). For both males and females, significant differences were found among the northerly (Bering Strait and St. Matthew) and southerly (southeast) regions. However, these differences were more pronounced for females (*Ho*: Bering Strait = southeast, $F = 25.35$, $p < 0.0001$) than for males (*Ho*: Bering Strait = southeast, $F = 5.53$, $p = 0.001$). Differences were also found between the southeast and St.
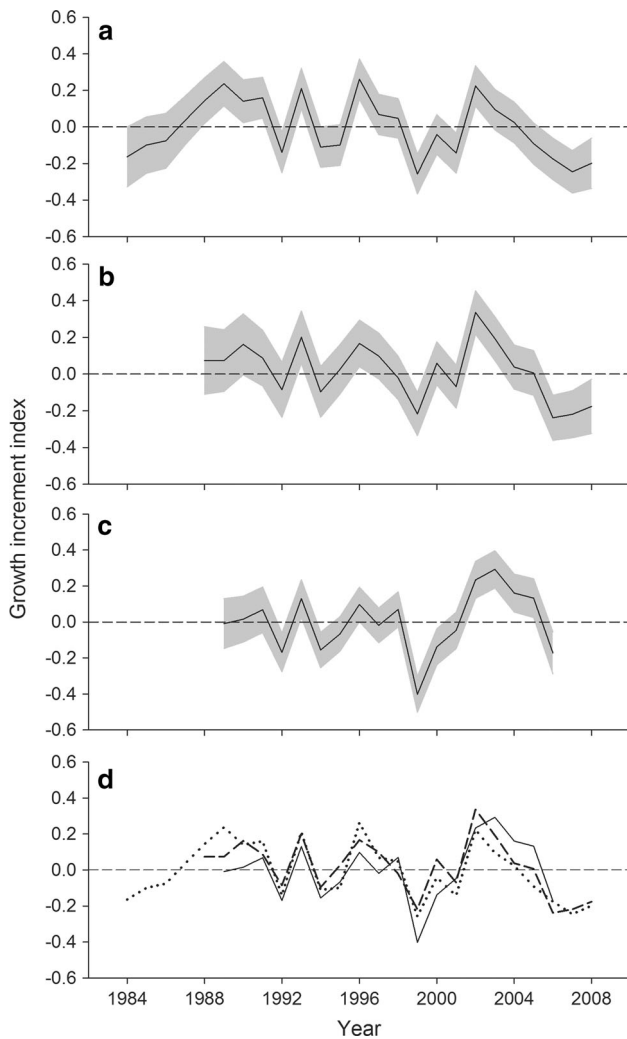
Fig. 3 Otolith biochronologies (*black lines*) with 95 % confidence intervals (*shaded area*) for yellowfin sole (*Limanda aspera*) collected from **a** Bering Strait, **b** St. Matthew, and **c** southeast Bering Sea; **d** Biochronologies for the three regions of interest (Bering Strait = *dotted line*, St. Matthew = *dashed line*, Southeast = *solid line*)
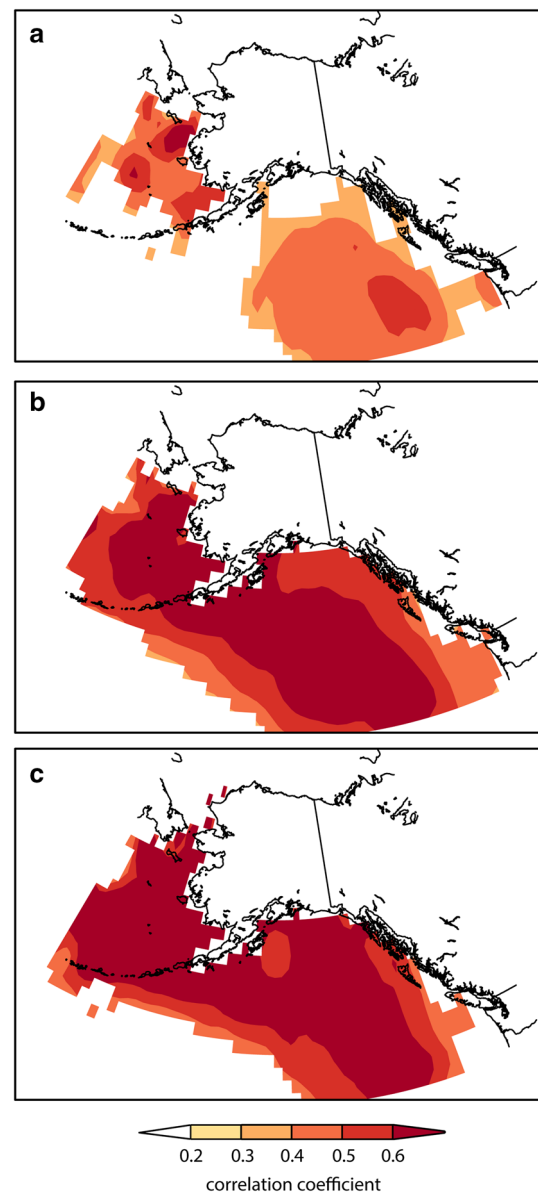

Fig. 4 Spatial correlations between gridded sea surface temperatures (SST) and the **a** Bering Strait, **b** St. Matthew, and **c** Southeast Bering Sea otolith biochronologies for yellowfin sole (*Limanda aspera*). Monthly SSTs (including lags of ±4 months into adjacent years) were correlated with each biochronology and averaged when highly significant ($p < 0.01$). The window (average) of highly significant months was April–November for the Bering Strait, April–March for St. Matthew, and Apr–Jan for Southeast. Maps show significant correlations ($p < 0.1$) between averaged SSTs and each biochronology

Matthew for both sexes (males $F = 6.80$, $p = 0.0002$; females $F = 7.24$, $p < 0.0001$), and between Bering Strait and St. Matthew for females ($F = 3.05$, $p = 0.03$) but not for males ($F = 1.23$, $p = 0.30$).

These results suggest that yellowfin sole in the more northerly regions grow to larger asymptotic sizes (L_∞) but at slower rates (K) than fish in the southeastern Bering Sea. For instance, $L_\infty = 486.1$ mm and $K = 0.086$ years^{-1} for female yellowfin sole near Bering Strait, compared to $L_\infty = 394.3$ mm and $K = 0.140$ years^{-1} in the southeastern Bering Sea (Table 4). These results are consistent with the otolith accretion rates from the mixed model biochronology analysis.

Discussion

By their very nature, otolith biochronologies represent time series data (repeated measures at the subject level) that possess a nested or hierarchical structure. Hierarchical or

Table 4 Von Bertalanffy growth parameter estimates for all yellowfin sole (*Limanda aspera*) collected from the Bering Strait (BS), St. Matthew (SM), and southeast Bering Sea (SE) regions during trawl surveys in 2010

Region	n	L_∞ mm	K (year^{-1})	t_0 (year)	σ_e^2
BS	42	399.2	0.113	0.581	754.4
		(357.0–441.4)	(0.083–0.142)	(−0.042 to 1.204)	
SM ♂	105	377.0	0.147	1.271	799.0
		(355.7–398.2)	(0.116–0.177)	(0.543 to 1.999)	
SE	260	350.1	0.168	0.860	588.7
		(341.8–358.5)	(0.153–0.184)	(0.542 to 1.179)	
BS	72	486.1	0.086	0.644	979.4
		(451.8–520.4)	(0.067–0.104)	(−0.114 to 1.401)	
SM ♀	124	447.4	0.108	0.703	644.6
		(422.3–472.5)	(0.092–0.124)	(0.264 to 1.141)	
SE	355	394.3	0.140	0.816	765.4
		(385.3–403.2)	(0.127–0.153)	(0.469 to 1.162)	

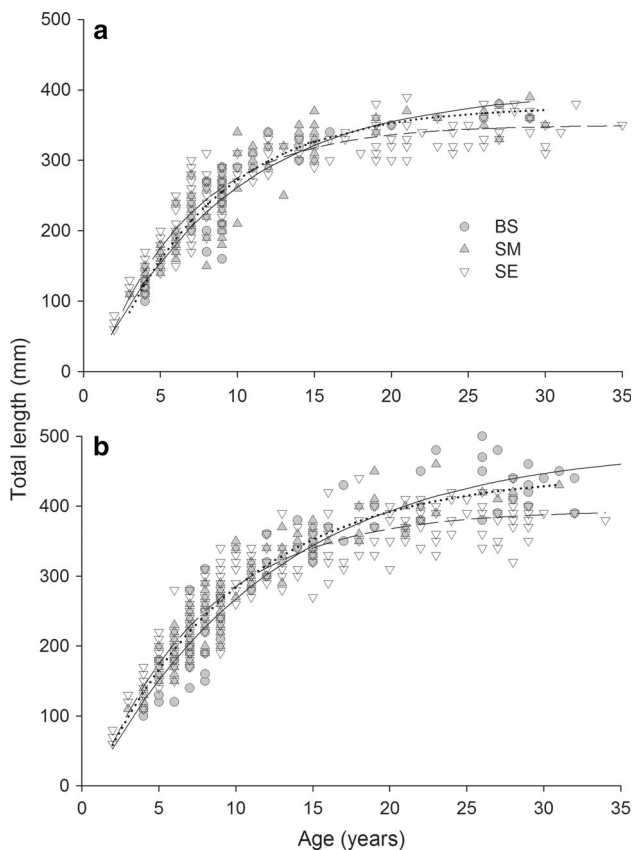95 % confidence intervals for each parameter estimate are given in parentheses

Fig. 5 Length-at-age data fitted with von Bertalanffy growth functions for **a** male and **b** female yellowfin sole (*Limanda aspera*) from Bering Strait (BS, *solid line*), St. Matthew (SM, *dotted line*), and southeast Bering Sea (SE, *dashed line*)

mixed effects models are appropriate for analyzing these data since they can simultaneously consider random individual variability, intrinsic fixed effects, and extrinsic environmental factors responsible for growth (Helser et al. 2012), as well as account for spatial and temporal autocorrelation (Morrongiello et al. 2012). Using this approach offers advantages over methods in which each measurement time series is detrended individually, especially in the case of short-lived individuals in which case low-frequency (long-term) climate effects on growth are highly prone to being lost (Cook et al. 1995; Helser et al. 2012; Morrongiello et al. 2012). Hierarchical or mixed effects modeling is most analogous to regional curve standardization (RCS) approaches, as has been employed to preserve low-frequency variability in dendroclimatology, and more recently, scleroclimatology studies (Helama et al. 2009; Butler et al. 2010; Briffa and Melvin 2011). Importantly, low-frequency variability is best preserved by using individuals collected across a range of years such that samples of different ages contribute to each calendar year in the biochronology (Briffa and Melvin 2011). Yet the hierarchical or mixed model approach preserves as much low-frequency variability as possible in this dataset, as would RCS, and facilitates direct comparisons among the properties of multiple datasets.

One limitation of our study was that we did not have adequate sample sizes to test for effects of sex or fish age at capture on otolith growth. Additionally, multiple otoliths were sometimes collected from the same haul and could thus potentially reflect more localized relationships with environmental conditions. However, each biochronology was summarized over a relatively large spatial scale, which likely minimizes the risk of bias. Environmental effects were not considered directly within the model, although this approach has been used in other studies (Helser et al. 2012; Morrongiello and Thresher 2015; von Biela et al. 2015). Given the range of regional environmental indices available and the fact that little is known regarding seasonal movements of yellowfin sole at northern latitudes, we chose instead to test for effects of temperature outside the model. Future work could include the proposal of a

mechanistic hypothesis of the effect of a suite of plausible environmental factors based on the findings presented here, which could then be tested explicitly within the framework of the statistical model. Notably, the Bering Strait chronology was not as strongly tied to local temperatures, indicating possible short-term residence at these relatively high latitudes.

In general, a high degree of synchrony was observed in otolith growth-increment widths both within and among regions, in spite of large geographical distances separating the three biochronologies (>600 km between the Bering Strait and Southeast biochronologies). The Southeast biochronology otoliths were collected over a wider area than the northern specimens (Fig. 1) but were found to crossdate well, with the highest series intercorrelation (Matta et al. 2010; Table 1). While the Bering Strait and St. Matthew intercorrelation values are slightly lower than that of the Southeast, they are still comparable to those published for other northeast Pacific taxa including rockfish (*Sebastes* spp.) (Black 2009) and fall within bounds considered acceptable by the dendrochronology community (Grissino-Mayer 2001; Black et al. 2005).

Despite general similarities in overall interannual trends in otolith growth, closer examination of the three biochronologies indicated subtle differences from one another. The highest degree of variability between individuals in growth response (represented by σ_h^2) was observed in the St. Matthew biochronology (Table 3). The biochronologies also differed from each other in amplitude; negative anomalies were generally greatest in the Southeast biochronology, whereas positive anomalies were greatest in the Bering Strait and St. Matthew biochronologies (Fig. 3). Differences in somatic growth were also detected among the regions (Fig. 5), such that mean length at age was generally greater with increasing latitude. Despite our small sample sizes for the Bering Strait and St. Matthew regions, this pattern of growth is consistent with findings by Nichol (1997), where fish from the southeastern Bering Sea shelf had smaller sizes at age than those located farther to the northwest.

Differences among the biochronologies were also revealed with respect to their relationships with environmental variables. Of the climate indices examined, temperature generally had the strongest relationships with the biochronologies. Contrary to our initial predictions, the Bering Strait biochronology did not exhibit a significant relationship with instrumental bottom temperatures in the northern Bering Sea. Rather, the Bering Strait biochronology was most closely related to bottom temperatures from the summer survey and the M2 mooring, both of which were located in the southeastern Bering Sea. Furthermore, the Bering Strait biochronology had the most spatially localized relationship with gridded SSTs and the narrowest window of months across which highly significant correlations were detected. These findings suggest that yellowfin sole from the three regions experience differential effects of climate across the latitudinal gradient, and in a manner contrary to our initial hypothesis that climate impacts would be strongest in the most northerly group. Indeed, the Bering Strait biochronology had the weakest relationships with temperature and ice cover, implying that growth there was under weaker climate control, or possibly that there was less interannual variability in oceanographic conditions in these northern latitudes.

Adult yellowfin sole in the eastern Bering Sea undergo complex annual migrations, over-wintering along the outer continental shelf presumably to avoid colder water temperatures and ice cover, and moving to the inner and middle continental shelf beginning in the spring and summer for the purposes of spawning and feeding (Bakkala 1981; Wakabayashi 1989; Wilderbuer et al. 1992). Three over-wintering groups of adults have been identified: a large group north of Unimak Island, a smaller group west of the Pribilof Islands, and a very small group south of the Pribilof Islands (Bakkala 1981; Wakabayashi 1989). While yellowfin sole in the eastern Bering Sea is genetically considered a single stock (Grant et al. 1983), there appears to be limited mixing between the Unimak and Pribilof groups during their inshore spawning migration (Wakabayashi 1989). Migration patterns of yellowfin sole in the northern Bering Sea are currently unknown. However, given the poorer climate–growth correlations we observed for the Bering Strait biochronology, it is possible they only reside there briefly in summer, retreating south during the fall and winter to avoid ice cover and associated colder temperatures. Such cold-water avoidance would be consistent with behavior of yellowfin sole observed on the southeastern Bering Sea shelf (Bakkala 1981; Wakabayashi 1989; Wilderbuer et al. 1992). More work is clearly needed to understand spawning habitat utilization and seasonal distribution of yellowfin sole in the northern Bering Sea, especially whether they are part of a known southern overwintering group or if they move elsewhere to avoid colder winter temperatures.

Oceanographic and ecological differences among the regions could explain some of the observed spatial variation in growth response. Ice cover varies in extent and duration between the northern and southern Bering Sea. Ice appears earlier and persists for a longer time at greater concentration in the northern Bering Sea, whereas the southern shelf exhibits higher year-to-year variability in sea-ice extent (Stabeno et al. 2012). Timing of thermal minima also differs between northern and southern Bering Sea mid-shelf bottom water, with the north reaching a minimum in late December or January, in contrast with February or March in the south (Stabeno et al. 2012).

Furthermore, late summer bottom temperatures in the north are cooler than those in the south (Stabeno et al. 2012). The northern and southern Bering Sea shelves are also quite different from each other in terms of community structure, with fish dominating the south and invertebrates dominating the north (Lauth 2011), and the benthos playing a far more important role in production and energy flow in the shallow high latitudes (Grebmeier et al. 1995).

Factors other than climate, such as competition and prey availability, may have an effect on growth in yellowfin sole. Primary prey items in the yellowfin sole diet are polychaetes, bivalves, gammarid amphipods, brittle stars, and sand dollars (Yang and Yeung 2013; Yeung and Yang 2014). Temperature is less important in explaining polychaete assemblages than seafloor sediment texture and composition (Yeung et al. 2010). As a result, there are regional differences in the yellowfin sole diet even within the southeastern Bering Sea; polychaetes are associated with the muddier middle shelf and thus are more prevalent in the diet of yellowfin sole collected there, whereas clams are more dominant in the diet of yellowfin sole collected from the sandier inner shelf (Yang and Yeung 2013). In contrast to the southern Bering Sea, where the diet of yellowfin sole corresponds directly with local prey species composition (Yeung et al. 2013), yellowfin sole in the northern Bering Sea appear to selectively prefer amphipods, which are relatively nutritionally rich (Yeung and Yang 2014). Given that yellowfin sole population density is lower in the northern Bering Sea (Nichol 1997; Lauth 2011), the benefit of energy-rich prey and reduced competition, along with possible transient habitat usage, may explain the apparent reduced sensitivity of yellowfin sole in that region to climate variability.

The mixed effects modeling approach used here simultaneously considered and partitioned variance among intrinsic and extrinsic factors responsible for growth, offering an advantage over traditional detrending methods. Furthermore, this approach allowed us to examine regional differences in growth and to quantify growth variability of yellowfin sole across its range in the eastern Bering Sea in the context of potential ecological and oceanographic drivers. Clearly, while growth of yellowfin sole follows the same general pattern throughout the eastern Bering Sea, a latitudinal gradient was apparent such that growth of individuals in the south is more tightly linked to climate than that of individuals in the north. As climate is predicted to change in the northern Bering Sea and Arctic regions, biochronologies such as these may be valuable tools to predict future biological responses, even in regions where impacts of climate change may not be felt uniformly across a species' range.

References

Bakkala RG (1981) Population characteristics and ecology of yellowfin sole. In: Hood DW, Calder JA (eds) The eastern Bering Sea shelf: oceanography and resources. US Dept Commer NOAA, Washington, DC, pp 553–574

Black BA (2009) Climate-driven synchrony across tree, bivalve, and rockfish growth-increment chronologies of the northeast Pacific. Mar Ecol Prog Ser 378:37–46. doi:10.3354/meps07854

Black BA, Boehlert GW, Yoklavich MM (2005) Using tree-ring crossdating techniques to validate annual growth increments in long-lived fishes. Can J Fish Aquat Sci 65:2277–2284. doi:10.1139/F05-142

Black BA, Schroeder ID, Sydeman WJ, Bograd SJ, Wells BK, Schwing FB (2011) Winter and summer upwelling modes and their biological importance in the California Current ecosystem. Global Change Biol 17:2536–2545. doi:10.1111/j.1365-2486.2011.02422.x

Black BA, Matta ME, Helser TE, Wilderbuer TK (2013) Otolith biochronologies as multidecadal indicators of body size anomalies in yellowfin sole (*Limanda aspera*). Fish Oceanogr 22(6):523–532. doi:10.1111/fog.12036

Black BA, Sydeman WJ, Frank DC, Griffin D, Stahle DW, García-Reyes M, Rykaczewski RR, Bograd SJ, Peterson WT (2014) Six centuries of variability and extremes in a coupled marine-terrestrial ecosystem. Science 345:1498–1502. doi:10.1126/science.1253209

Briffa KR, Melvin TM (2011) A closer look at regional curve standardization of tree-ring records: justification of the need, a warning of some pitfalls, and suggested improvements in its application. In: Hughes MK, Diaz HF, Swetnam TW (eds) Dendroclimatology: developments in paleoenvironmental research, vol 11, pp 553–574

Burnham KP, Anderson DR (2002) Model selection and multimodel inference: a practical information-theoretic approach, 2nd edn. Springer, New York

Butler PG, Richardson CA, Scourse JD, Wanamaker AD Jr, Shammon TM, Bennell JD (2010) Marine climate in the Irish Sea: analysis of a 489-year marine master chronology derived from growth increments in the shell of the clam *Arctica islandica*. Quat Sci Rev 29:1614–1632. doi:10.1016/j.quascirev.2009.07.010

Carilli JE, Norris RD, Black B, Walsh SM, McField M (2010) Century-scale records of coral growth rates indicate that local stressors reduce coral thermal tolerance threshold. Global Change Biol 16:1247–1257. doi:10.1111/j.1365-2486.2009.02043.x

Cook ER, Briffa KR, Meko DM, Graybill DA, Funkhouser G (1995) The 'segment length curse' in long tree-ring chronology development for palaeoclimatic studies. Holocene 5(2):229–237. doi:10.1177/095968369500500211

Fritts HC (1976) Tree rings and climate. Academic Press, New York

Gillanders BM, Black BA, Meekan MG, Morrison MA (2012) Climatic effects on the growth of a temperate reef fish from the Southern Hemisphere: a biochronological approach. Mar Biol 159:1327–1333. doi:10.1007/s00227-012-1913-x

Grant WS, Bakkala R, Utter FM, Teel DJ, Kobayashi T (1983) Biochemical genetic population structure of yellowfin sole, *Limanda aspera*, of the North Pacific Ocean and Bering Sea. Fish Bull 81(4):667–677. http://fishbull.noaa.gov/81-4/grant.pdf

Grebmeier JM, Smith Jr WO, Conover RJ (1995) Biological processes on Arctic continental shelves: ice-ocean-biotic interactions. In: Smith WO, Grebmeier JM (eds) Arctic oceanography: marginal ice zones and continental shelves. Coastal and Estuarine Studies 49, Washington DC, American Geophysical Union, pp 231–261

Grissino-Mayer HD (2001) Evaluating crossdating accuracy: a manual and tutorial for the computer program COFECHA. Tree Ring Res 57:205–221

Helama S, Schöne BR, Black BA, Dunca E (2006) Constructing long-term proxy series for aquatic environments with absolute dating control using a sclerochronological approach: introduction and advanced applications. Mar Freshw Res 57:591–599. doi:10.1071/MF05176

Helama S, Nielsen JK, Macias Fauria M, Valovirta I (2009) A fistful of shells: amplifying sclerochronological and palaeoclimate signals from molluscan death assemblages. Geol Mag 146:917–930. doi:10.1017/S0016756809990033

Helser TE, Lai H-L (2004) A Bayesian hierarchical meta-analysis of fish growth: with an example for North American largemouth bass, *Micropterus salmoides*. Ecol Model 178:399–416. doi:10.1016/j.ecolmodel.2004.02.013

Helser TE, Lai H-L, Black BA (2012) Bayesian hierarchical modeling of Pacific geoduck growth increment data and climate indices. Ecol Model 247:210–220. doi:10.1016/j.ecolmodel.2012.08.024

Hollowed AB, Planque B, Loeng H (2013) Potential movement of fish and shellfish stocks from the sub-Arctic to the Arctic Ocean. Fish Oceanogr 22:355–370. doi:10.1111/fog.12027

Holmes RL (1983) Computer-assisted quality control in tree-ring dating and measurement. Tree Ring Bull 43:69–78

IPCC (2014) Climate change 2014: synthesis report. Contribution of Working Groups I, II and III to the fifth assessment report of the Intergovernmental Panel on Climate Change [Core Writing Team, Pachauri RK, Meyers LA (eds)]. IPCC, Geneva, Switzerland. http://www.ipcc.ch

Kimura DK, Anderl DM, Goetz BJ (2007) Seasonal marginal growth on otoliths of seven Alaska groundfish species support the existence of annual patterns. Alaska Fish Res Bull 12(2):243–251. http://www.sf.adfg.state.ak.us/FedAidPDFs/AFRB.12.2.243-251.pdf

Lauth RR (2011) Results of the 2010 eastern and northern Bering Sea continental shelf bottom trawl survey of groundfish and invertebrate fauna. NOAA Tech Memo NMFS-AFSC-227. http://www.afsc.noaa.gov/Publications/AFSC-TM/NOAA-TM-AFSC-227.pdf

Matta ME, Goetz BJ (2012) Otolith growth pattern interpretation. In: Matta ME, Kimura DK (eds) Age determination manual of the Alaska Fisheries Science Center Age and Growth Program. NOAA Professional Paper NMFS 13, pp 5–10. http://spo.nwr.noaa.gov/pp13.pdf

Matta ME, Black BA, Wilderbuer TK (2010) Climate-driven synchrony in otolith growth-increment chronologies for three Bering Sea flatfish species. Mar Ecol Prog Ser 413:137–145. doi:10.3354/meps08689

Morrongiello JR, Thresher RE (2015) A statistical framework to explore ontogenetic growth variation among individuals and populations: a marine fish example. Ecol Monogr 85(1):93–115. doi:10.1890/13-2355.1

Morrongiello JR, Thresher RE, Smith DC (2012) Aquatic biochronologies and climate change. Nat Clim Change 2:849–857. doi:10.1038/nclimate1616

Nichol DG (1997) Effects of geography and bathymetry on growth and maturity of yellowfin sole, *Pleuronectes asper*, in the eastern Bering Sea. Fish Bull 95:494–503

NOAA (2014) Bering Sea climate. http://www.beringclimate.noaa.gov. Accessed 8 May 2014

Overland JE, Wang M (2013) When will the summer Arctic be nearly sea ice free? Geophys Res Lett 40:1–5. doi:10.1002/grl.50316

Rayner NE, Parker DE, Horton EB, Folland CK, Alexander LV, Rowell DP (2003) Global analyses of sea surface temperature, sea ice, and night marine air temperature since the late nineteenth century. J Geophys Res. doi:10.1029/2002JD002670

Shockley W, Matta ME (2012) Yellowfin sole (*Limanda aspera*). In: Matta ME, Kimura DK (eds) Age determination manual of the Alaska Fisheries Science Center Age and Growth Program. NOAA Professional Paper NMFS 13, pp 77–84. http://spo.nwr.noaa.gov/pp13.pdf

Stabeno PJ, Farley Jr Ed, Kachel NB, Moore S, Mordy CW, Napp JM, Overland JE, Pinchuk AI, Sigler MF (2012) A comparison of the physics of the northern and southern shelves of the eastern Bering Sea and some implications for the ecosystem. Deep Sea Res II 65–70:14–30. doi:10.1016/j.dsr2.2012.02.019

von Bertalanffy L (1938) A quantitative theory of organic growth (inquiries on growth laws II). Hum Biol 10(2):181–213

von Biela VR, Kruse GH, Mueter FJ, Black BA, Douglas DC, Helser TE, Zimmerman CE (2015) Evidence of bottom-up limitations in nearshore marine systems based on otolith proxies of fish growth. Mar Biol 162:1019–1031. doi:10.1007/s00227-015-2645-5

Wakabayashi K (1989) Studies on the fishery biology of yellowfin sole in the eastern Bering Sea [in Japanese, English summary]. Bull Far Seas Fish Res Lab 26:21–152

Weisberg S, Spangler G, Richmond LS (2010) Mixed effects models for fish growth. Can J Fish Aquat Sci 67:269–277. doi:10.1139/F09-181

Wilderbuer TK, Walters GE, Bakkala RG (1992) Yellowfin sole, *Pleuronectes asper*, of the eastern Bering Sea: biological characteristics, history of exploitation, and management. Mar Fish Rev 54(4):1–18. http://spo.nmfs.noaa.gov/mfr544/mfr5441.pdf

Wilderbuer TK, Nichol DG, Ianelli J (2015) Assessment of the yellowfin sole stock in the Bering Sea and Aleutian Islands. In: Stock assessment and fishery evaluation report for the groundfish resources of the Bering Sea/Aleutian Islands regions. Compiled by the Plan Team for the Groundfish Fisheries of the Bering Sea and Aleutian Islands, North Pacific Fishery Management Council, Anchorage, AK, pp 733–820. http://www.afsc.noaa.gov/REFM/Docs/2015/BSAIyfin.pdf

Woodgate RA, Aagaard K, Weingartner TJ (2005) Monthly temperature, salinity and transport variability of the Bering Strait throughflow. Geophys Res Lett 32(4)

Yang M-S, Yeung C (2013) Habitat-associated diet of some flatfish in the southeastern Bering Sea. US Dep Commer, NOAA Tech Memo NMFS-AFSC-246. http://www.afsc.noaa.gov/publications/afsc-tm/noaa-tm-afsc-246.pdf

Yeung C, Yang M-S (2014) Habitat and infauna prey availability for flatfishes in the northern Bering Sea. Polar Biol 37:1769–1784. doi:10.1007/s00300-014-1560-4

Yeung C, Yang M-S, McConnaughey RA (2010) Polychaete assemblages in the south-eastern Bering Sea: linkage with groundfish distribution and diet. J Mar Biol Assoc UK 90(5):903–917. doi:10.1017/S002531541000024X

Yeung C, Yang M-S, Jewett SC, Naidu AS (2013) Polychaete assemblage as surrogate for prey availability in assessing southeastern Bering Sea flatfish habitat. J Sea Res 76:211–221. doi:10.1016/j.seares.2012.09.008